

## SUPPLEMENTARY INFORMATION - Rudolf et al

**Supplementary Table 1.** Data collection, phasing and refinement statistics

	PTCH1 <sub>ECD1</sub> - NB64 S-SAD	PTCH1 <sub>ECD1</sub> - NB64 native	PTCH1 <sub>ECD1</sub> - NB64-CHS	PTCH1 <sub>ECD1</sub>	PTCH1 <sub>ECD2</sub> - NB75
<b>Data collection</b>					
Space group	<i>P</i> 2 <sub>1</sub> 2 <sub>1</sub> 2 <sub>1</sub>	<i>P</i> 2 <sub>1</sub> 2 <sub>1</sub> 2 <sub>1</sub>	<i>P</i> 2 <sub>1</sub> 2 <sub>1</sub> 2 <sub>1</sub>	<i>P</i> 2 <sub>1</sub> 2 <sub>1</sub> 2 <sub>1</sub>	<i>P</i> 2 <sub>1</sub> 2 <sub>1</sub> 2 <sub>1</sub>
Cell dimensions					
<i>a</i> , <i>b</i> , <i>c</i> (Å)	48.1, 67.2, 150.4	47.7, 65.9, 150.5	47.3, 65.7, 151.4	49.2, 65.7, 100.3	76.2, 101.1, 106.2
$\alpha$ , $\beta$ , $\gamma$ (°)	90.0, 90.0, 90.0	90.0, 90.0, 90.0	90.0, 90.0, 90.0	90.0, 90.0, 90.0	90.0, 90.0, 90.0
Resolution (Å)	75.18-2.79 (2.94-2.79)	150.54-2.10 (2.14-2.10)	37.19-1.90 (1.95-1.90)	50.14-1.95 (1.99-1.95)	39.16-2.20 (2.26-2.20)
<i>R</i> <sub>merge</sub>	0.116 (>1)	0.066 (>1)	0.111 (>1)	0.129 (>1)	0.164 (>1)
<i>R</i> <sub>pim</sub>	0.031 (0.817)	0.027 (0.696)	0.053 (0.867)	0.055 (0.525)	0.059 (0.722)
<i>CC</i> <sub>1/2</sub>	0.999 (0.462)	0.998 (0.521)	0.998 (0.360)	0.998 (0.316)	0.997 (0.391)
<i>I</i> / $\sigma$ <i>I</i>	22.2 (1.1)	16.2 (1.7)	9.1 (0.8)	10.7 (1.4)	9.8 (1.1)
Unique reflections	11497 (1387)	27821 (1068)	37866 (2618)	24282 (1168)	42185 (3069)
Completeness (%)	90.9 (77.1)	97.5 (75.5)	99.4 (94.9)	100.0 (99.1)	99.7 (99.3)
Redundancy	25.9 (24.2)	11.8 (7.8)	5.2 (4.2)	6.4 (5.7)	8.6 (8.3)
<b>Refinement</b>					
Resolution (Å)		50.00-2.10 (2.17-2.10)	37.19-1.90 (1.95-1.90)	50.19-1.95 (2.00-1.95)	39.19-2.20 (2.26-2.20)
No. reflections		25995 (1423)	37775 (2584)	23043 (1666)	40108 (2909)
<i>R</i> <sub>work</sub> / <i>R</i> <sub>free</sub>		21.8/25.5 (41.1/37.7)	18.7/22.8 (33.7/34.9)	19.9/25.5 (35.0/36.1)	20.4/24.1 (32.6/36.8)
No. atoms					
Protein		3150	3166	2153	5107
Ligand/ion		42	77	28	47
Water		84	210	99	202
<i>B</i> -factors					
Protein		75	42	39	63
Ligand/ion		120	74	81	98
Water		63	46	39	60
R.m.s deviations					
Bond lengths (Å)		0.010	0.008	0.008	0.008
Bond angles (°)		1.536	1.444	1.483	1.455

\*Highest-resolution shell is shown in parentheses.

**Supplementary Table 2.** Quality indication of the rebuilt PTCH1<sub>TM</sub>-pShhNc structure

	Re-refined model (PDB 6RVD)	Original model (PDB 6E1H)
<b>MODEL</b>		
No. atoms:		
Protein	16911	16647
Ligand/	258	20
RMSD lengths (Å)	0.008	0.008
RMSD angles (°)	1.106	1.173
Ramachandran (%):		
Favoured	95.39	90.09
Allowed	4.61	9.86
Outliers	0.00	0.05
Rotamer outliers (%)	0.06	1.76
CaBLAM outliers (%)	3.02	5.90
Clashscore (all atoms)	5.94	5.83
MolProbity score	1.65	2.05
<b>MODEL vs. DATA</b>		
EMRinger score	2.75	2.52
dFSC model (0.0/0.143/0.5)	3.23/3.44/3.89	3.26/3.45/3.89
Overall correlation		
coefficients:		
CC (mask)	0.79	0.75
CC (box)	0.60	0.60
CC (volume)	0.78	0.74
CC (peaks)	0.49	0.50
CC (main chain)	0.78	0.76
CC (side chain)	0.75	0.72

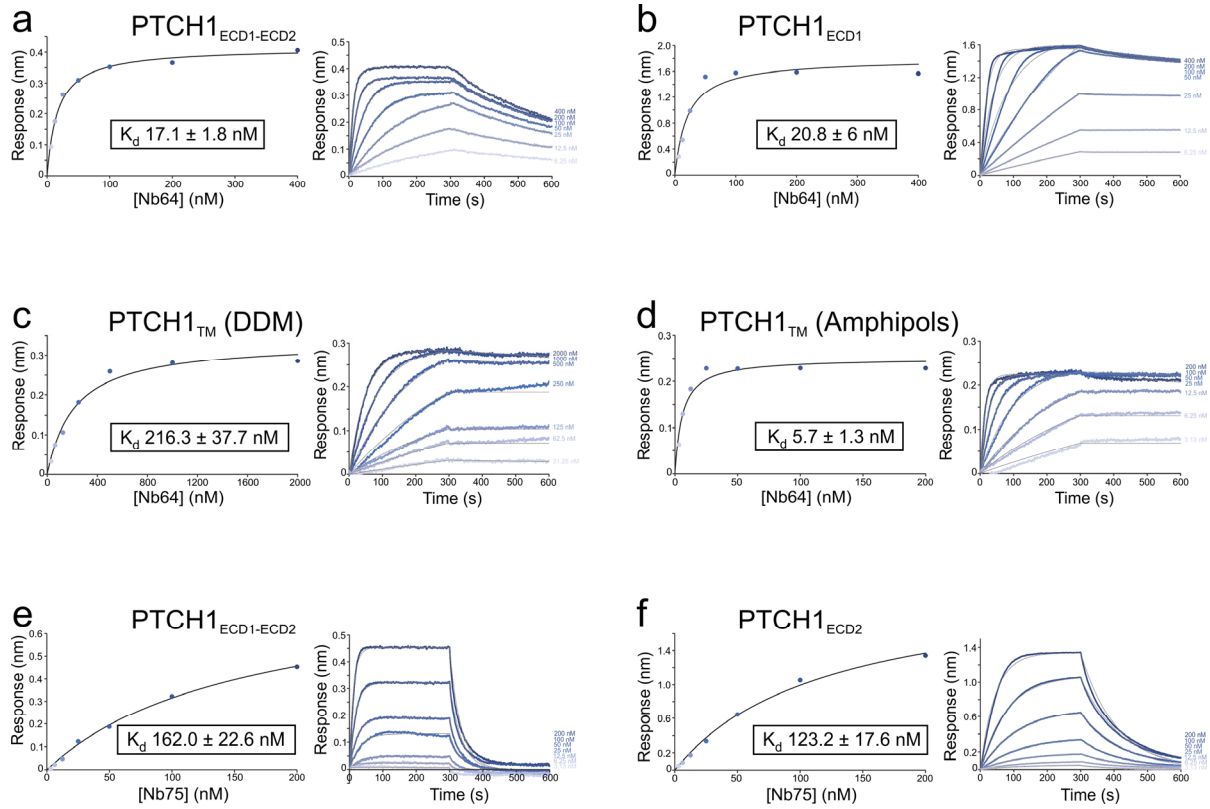
**Supplementary Table 3.** Exit points of tunnels identified over atomistic simulation of the PTCH1<sub>ECD</sub>-cholesterol complexes

Tunnel Exit	% of total tunnels	
	PTCH1 <sub>ECD</sub> mol-A	PTCH1 <sub>ECD</sub> mol-B
SBD sterol binding pocket	88.3	0.0
Side Exit 1	2.1	55.1
Side Exit 2	2.7	9.9
TM3 exit	4.7	0.7
TM12 exit	0.8	20.9
TM8	0.0	0.4
TM6	0.2	8.6
Other	1.2	4.4

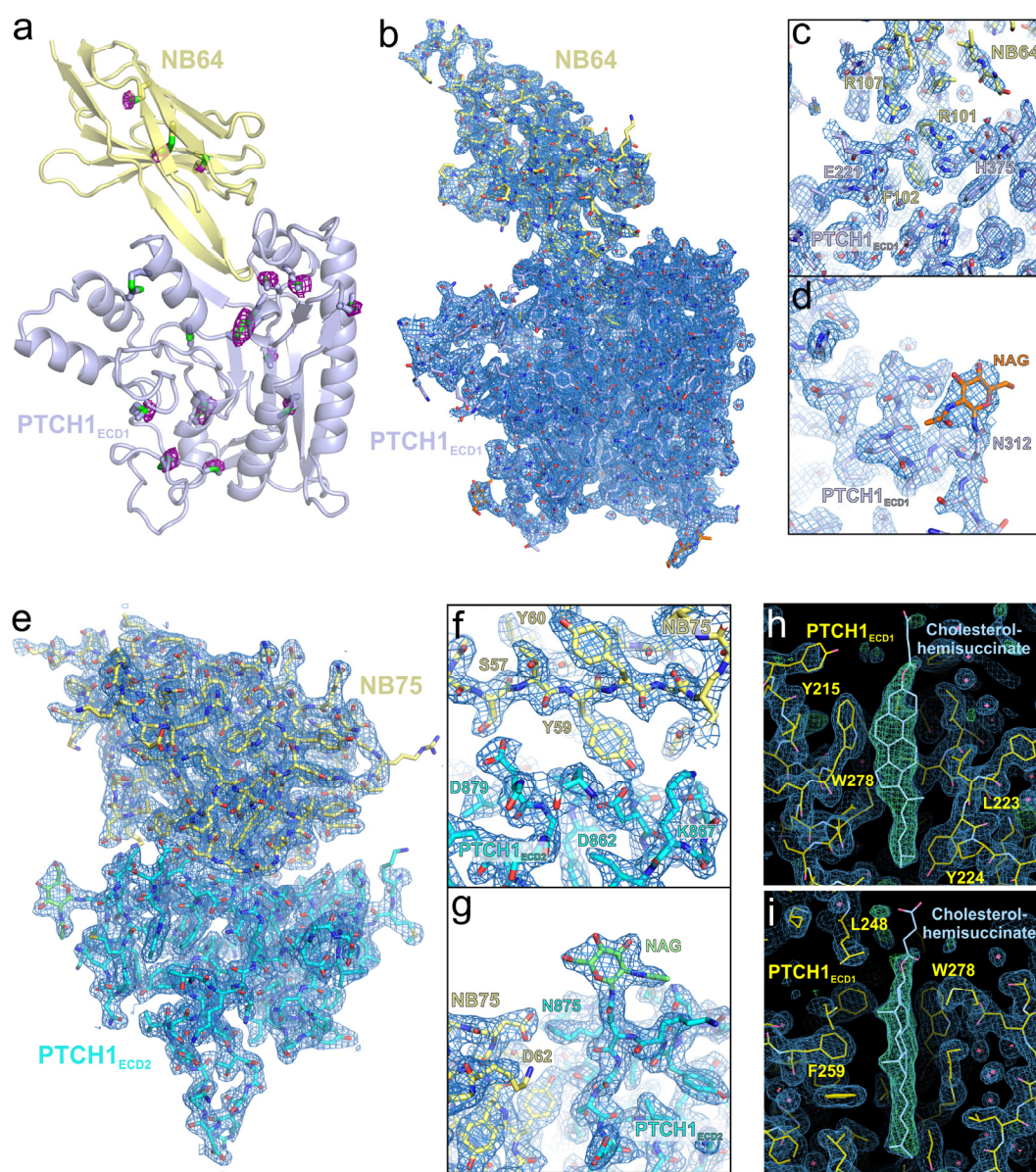
**Supplementary Table 4.** Non-standard pKa values of residues identified using PROPKA. Glutamate, aspartate and histidine residues with predicted pKa values greater than pH 7 are listed. Residues involved in the conserved putative ion binding motif are indicated (\*). These pKa values were not included in MD simulations for the listed constructs.

<b>Construct</b>	<b>Residue</b>	<b>Predicted pKa</b>
PTCH <sub>ECD</sub> -molA	GLU340	7.58
	HIS289	7.47
PTCH <sub>ECD</sub> -molB	GLU126	7.69
	HIS289	7.48
	HIS336	7.8
PTCH1 <sub>TM</sub>	ASP233	7.28
	ASP513*	8.45
	ASP514*	8.74
	GLU131	7.24
	GLU1095*	12.14
	HIS289	7.28
	HIS336	8.32

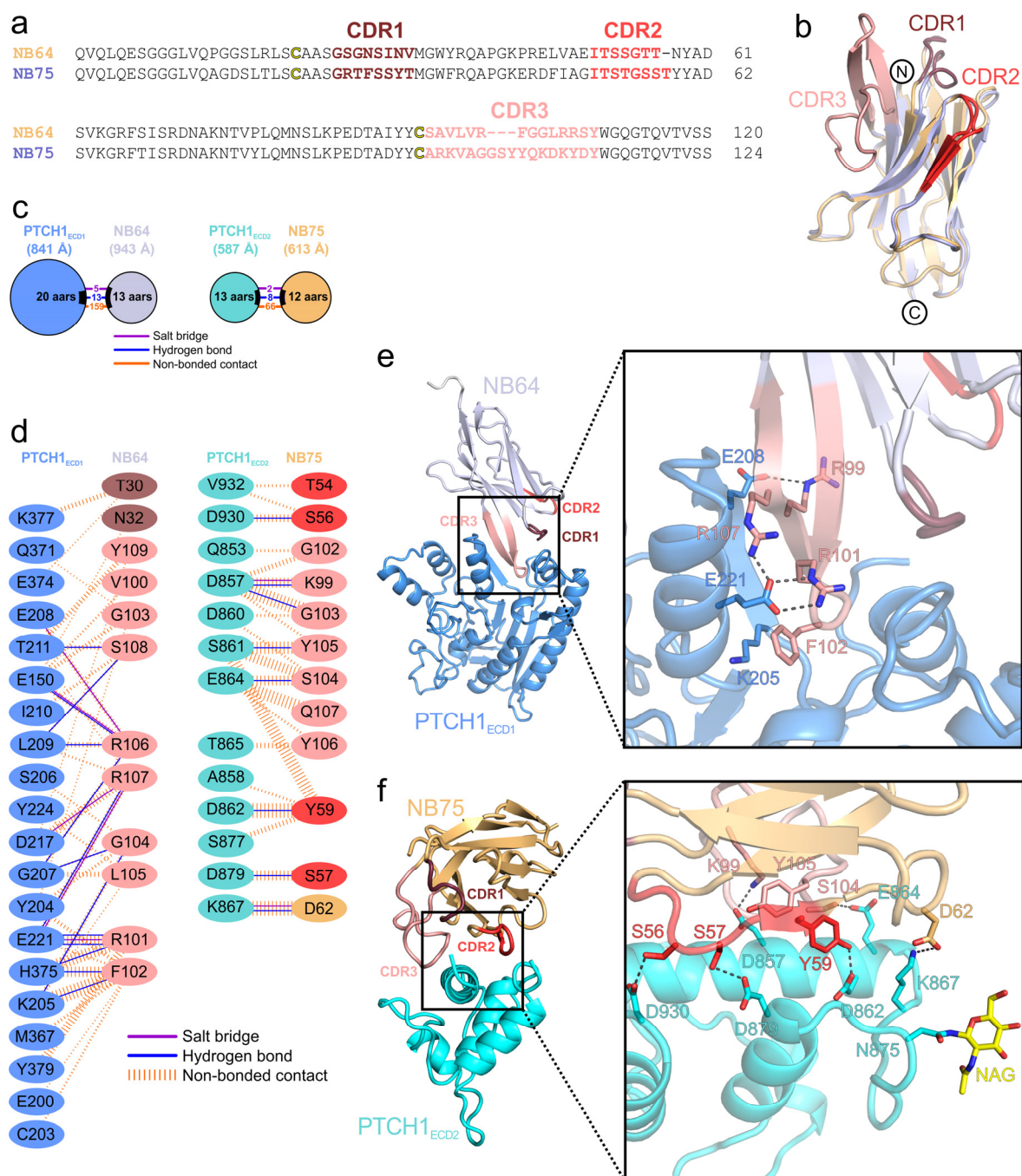




**Supplementary Figure 1: Characterization of the interactions between various PTCH1 constructs (shown and named in Fig. 1b) and nanobodies NB64 and NB75, respectively.** Bio-layer interferometry (BLI) multi-cycle kinetic measurements of the interaction between nanobody-64 (NB64, **a-d**) and nanobody-75 (NB75, **e and f**) with PTCH1<sub>ECD1-ECD2</sub>, PTCH1<sub>ECD1</sub>, PTCH1<sub>ECD2</sub> or a functional PTCH1 variant containing the TMD (PTCH1<sub>TM</sub>). For each panel, steady-state analysis to determine the equilibrium dissociation constant is shown on the left and real-time sensorgrams for association and dissociation at various NB concentrations are shown on the right. NB64 bound to the isolated PTCH1<sub>ECD1</sub> (**b**) and NB75 to the isolated PTCH1<sub>ECD2</sub> (**f**) with nanomolar affinity. While NB64 could also interact with PTCH1<sub>TM</sub> reconstituted with either detergent (**c**) or amphipols (**d**), NB75 showed no binding (not shown), suggesting that the NB75 epitope on PTCH1<sub>ECD2</sub> may not be exposed in the context of a PTCH1 protein containing both the TMD and the ECDs. BLI experiments were independently repeated 3 times with similar results.

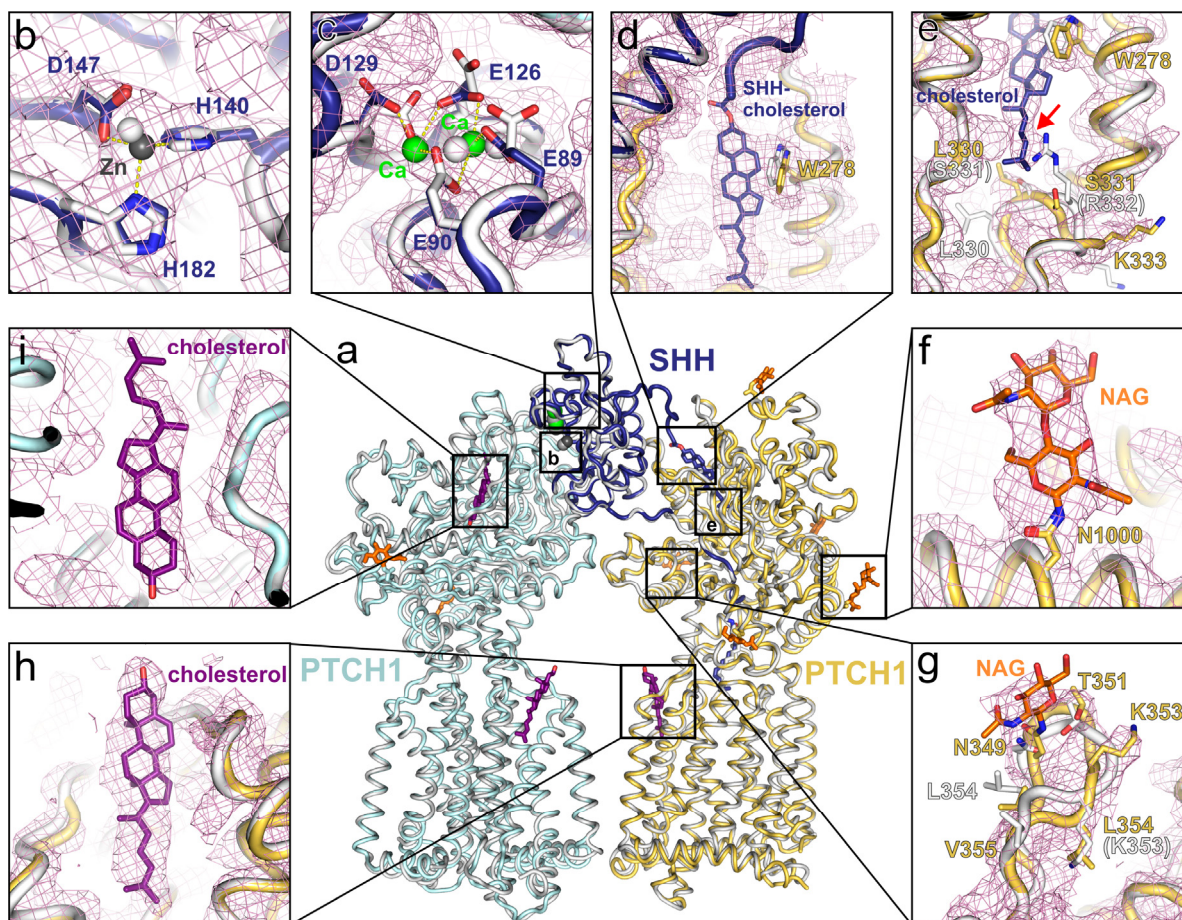


**Supplementary Figure 2: Structure solution of the PTCH1<sub>ECD1</sub>-NB64 and PTCH1<sub>ECD2</sub>-NB75 complexes.** **a**, Anomalous difference Fourier map (magenta mesh) calculated for the PTCH1<sub>ECD1</sub>-NB64 complex in the crystallographic asymmetric unit contoured at 4 $\sigma$  and mapped on the final refined model. The location of 14 out of 21 theoretical sulphur atoms could be determined and used for phasing. **b-d**, the 2.1 Å resolution sigma-weighted 2Fo-Fc map of the PTCH1<sub>ECD1</sub>-NB64 complex at 1 $\sigma$  after the final round of refinement using REFMAC<sup>1</sup>. **e-g**, 2.2 Å resolution sigma-weighted 2Fo-Fc map of the PTCH1<sub>ECD2</sub>-NB75 complex for one of the three copies present in the crystallographic asymmetric unit at 1 $\sigma$  after the final round of refinement using AutoBUSTER<sup>2</sup>. Both complex structures were determined to high quality revealing excellent map features, as shown by the N-linked glycans at asparagine-312 (d) and -875 (g). **h and i**, Close-up view of the cholesterol-hemisuccinate (HS) binding site in the PTCH1<sub>ECD1</sub>-NB64-cholesterol-HS complex. Sigma-weighted 2Fo-Fc at 1.9 Å resolution (contour level 1  $\sigma$ , blue) and Fo-Fc (contour level +3  $\sigma$ , green) maps from REFMAC<sup>1</sup> with omitted cholesterol-HS are shown.

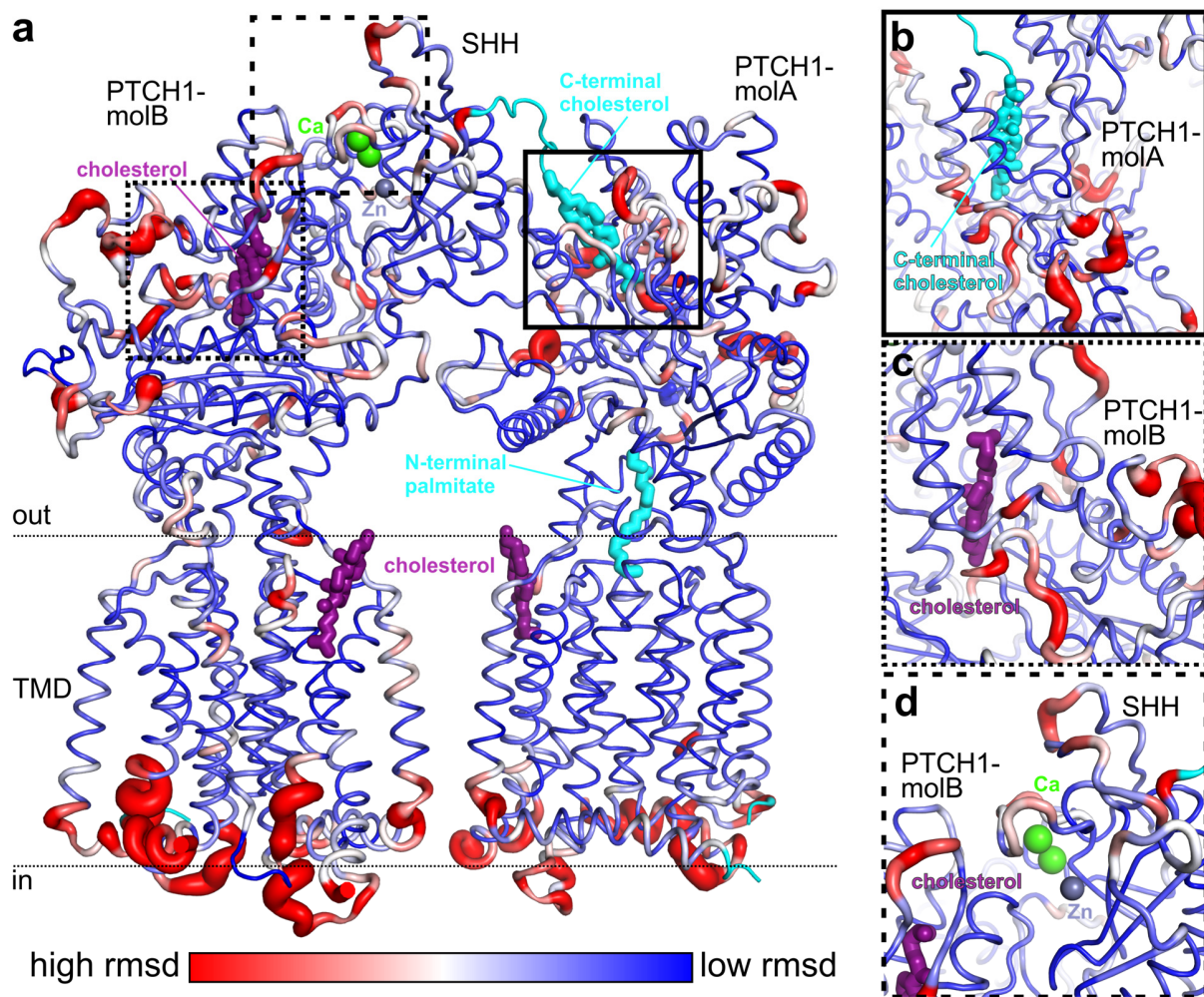


**Supplementary Figure 3: Structural characterisation of the PTCH1<sub>ECD1</sub>-NB64 and PTCH1<sub>ECD2</sub>-NB75 interactions.** **a**, Sequence alignment of nanobodies NB64 and NB75 with the complementary determining regions (CDRs) highlighted. **b**, Structural superposition of NB64 and NB75 using the colour-coding from **a**. **c** and **d**, Schematics of the PTCH1<sub>ECD1</sub>-NB64 and PTCH1<sub>ECD2</sub>-NB75 interactions adapted from PDBSUM<sup>3</sup>. The buried surface area of the respective protein in the complex is shown in brackets in **c**. Colour-coding is as in **Fig.1b** and **1c**. **e** and **f**, Cartoon presentations of the PTCH1<sub>ECD1</sub>-NB64 (**e**) and PTCH1<sub>ECD2</sub>-NB75 (**f**) complexes. Right panels show close-up views of the binding interfaces. Colour-coding is as in **d**. NB75 interacts with PTCH1 mainly via CDR2 (red) and CDR3 whereas NB64 almost exclusively uses CDR3, which punctures the PTCH1 surface and participates in formation of a new  $\beta$ -sheet.



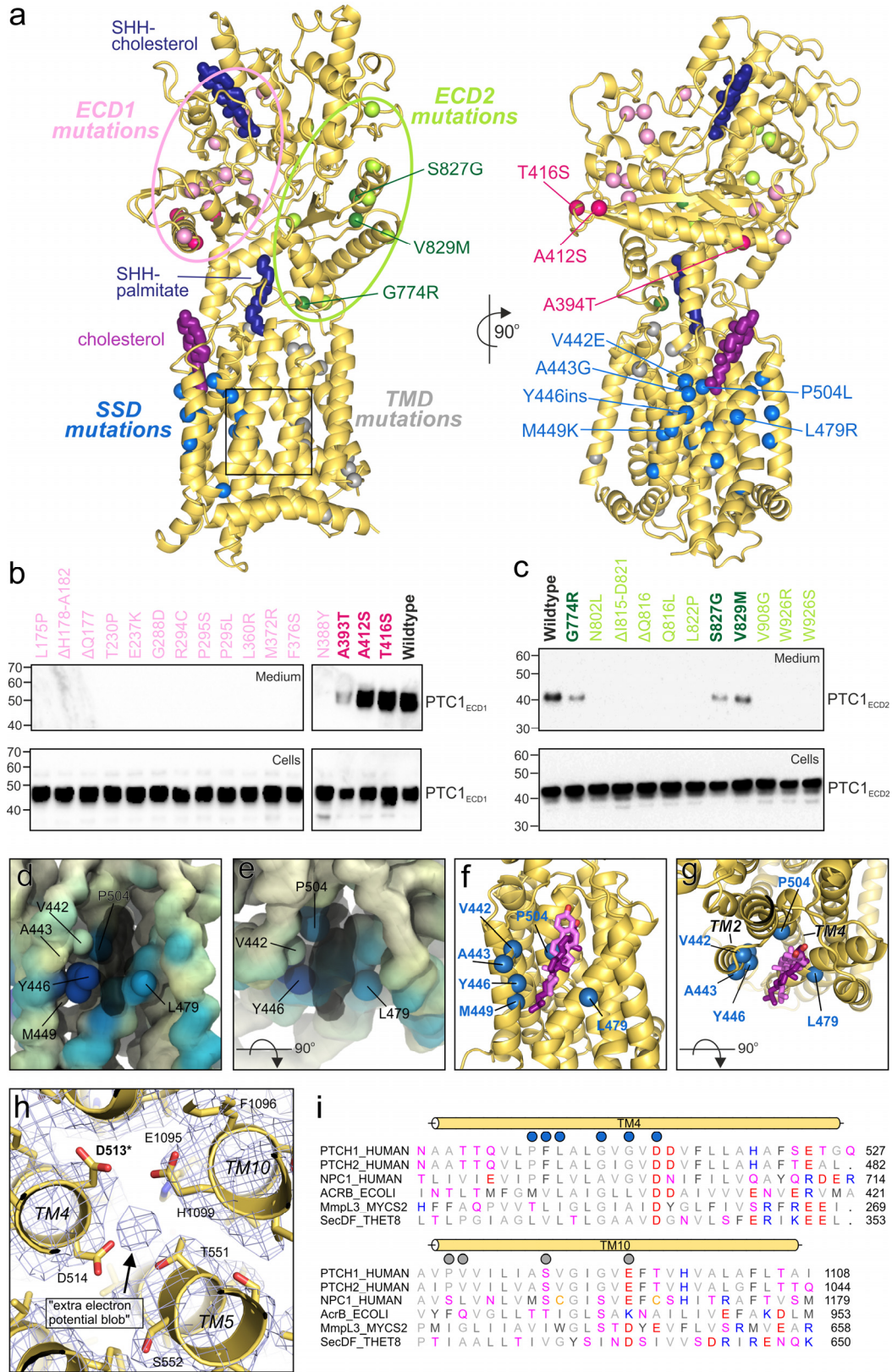


**Supplementary Figure 4: Re-refinement and enhancement of the previously deposited PTCH1-pShhNc cryo-EM structure.** **a**, Superposition of our revised PTCH1-pShhNc complex model (colour-coding and orientation as in Fig. 2a) and the previously deposited model (PDB Id. 6E1H<sup>4</sup>, grey). **b-i**, Close-up views of the selected regions. The previously deposited 3.5 Å cryo-EM map (EMD-8955<sup>4</sup>) linked to PDB entry 6E1H is shown as magenta mesh. **b and c**, the conserved SHH zinc (**b**) and calcium (**c**) binding sites. Both sites have previously been shown to be essential for SHH interactions with their receptors<sup>5-8</sup>. **d**, The cholesterol-modified C-terminus of pShhNc, which is absent from pdb Id. 6E1H<sup>4</sup>. There is clear extra electron density for the connection between the SHH core domain and the cholesterol. **e**, The lower lobe of the cholesterol binding site. In PDB 6E1H, this region is mistraced (e.g. R332 would wrongly occupy the cholesterol density) and is now corrected in our improved model. **f and g**, N-linked glycans at positions N1000 (**f**) and N349 (**g**). The N-acetylglucosamine moieties, clearly visible in the EMD-8955<sup>4</sup> map, were omitted in the original pdb file, but built in our model. This analysis also allowed us to re-trace the loop region around NAG-N349 (**g**). **h and i**, Putative cholesterol molecules located in the PTCH1-SSD (**h**) and PTCH1<sub>ECD1</sub> (**i**) not built in PDB 6E1H, but reported previously<sup>4,9-11</sup>. While we cannot entirely exclude the possibility that all the differences between our crystal structure and the original cryo-EM structure are due to differences in the environments in which the structures were determined, this figure shows several examples of how the optimized model, based on the crystal structure, allows better positioning of several side chains, cholesterol ligands and N-linked sugars. In addition, the RMSD for the comparison between the PTCH1-ECD1 crystal structure (complexed to cholesterol-HS) and ECD1 in the optimized cryo-EM molA (RMSD of 0.95 Å for the Ca positions of residues 155-423) is lower than for the comparison with molB (RMSD of 1.4 Å for the same Ca positions), which is reassuring given that both the PTCH1-ECD1 crystal structure and PTCH1-molA contain cholesterol in the same "hydroxyl-up" orientation.

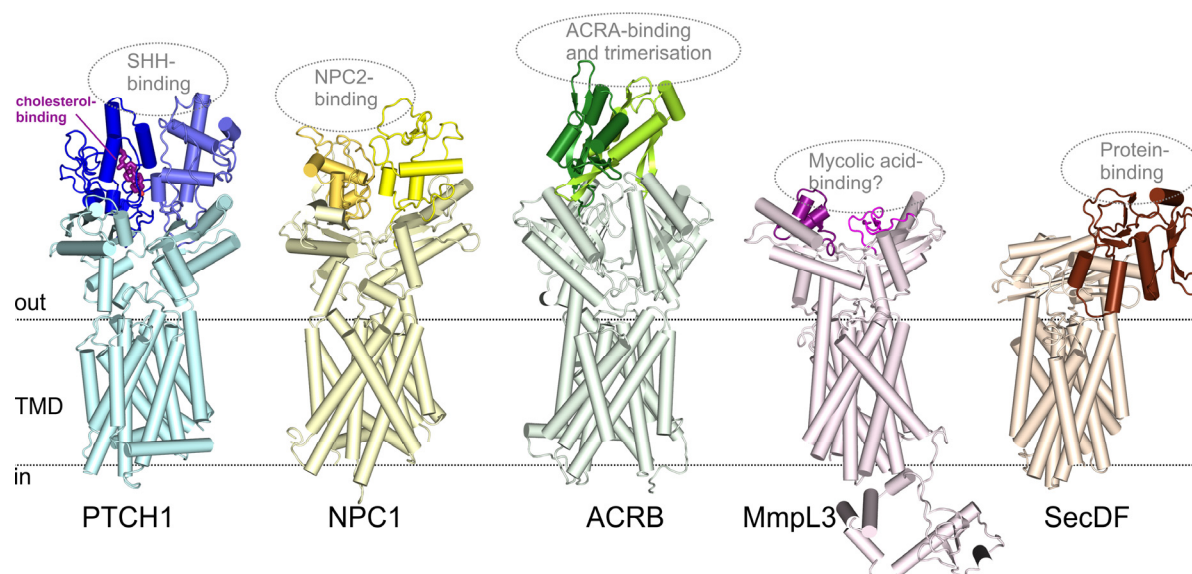


**Supplementary Figure 5: Structural comparison of our extended PTCH1 model and the original model (PDB Id. 6E1H<sup>4</sup>).** **a**, Overall structure of the extended 2:1 PTCH1:SHH complex. Colour-coding is according to rmsd deviation between our and the original PTCH1:SHH model (overall rmsd: 0.38 Å for 1641 equivalent Ca positions) calculated and visualized using program PYMOL (from red (high rmsd) to blue (low rmsd)). The SHH palmitoyl and cholesteryl moieties are coloured cyan, free cholesterol molecules are shown in sticks and coloured magenta. The calcium (green) and zinc (grey) ions are depicted as spheres. **b-d**, Close-up views of the PTCH1-molA (**b**) and PTCH1-molB (**c**) SBDs, and the SHH-PTCH1-molB interface that involves the SHH Ca and Zn binding sites (**d**). The major differences between our extended model and the original PDB 6E1H are located in the upper regions of PTCH1<sub>ECD1</sub> and PTCH1<sub>ECD2</sub> (especially in the SBDs of both PTCH1-molA and -molB, and the SHH-PTCH1-molB interface), and in the intracellular membrane proximal region. We note that the rmsd of the new model against 6E1H correlates with the lower resolution regions from the local resolution plot of the original cryo-EM map<sup>4</sup>.



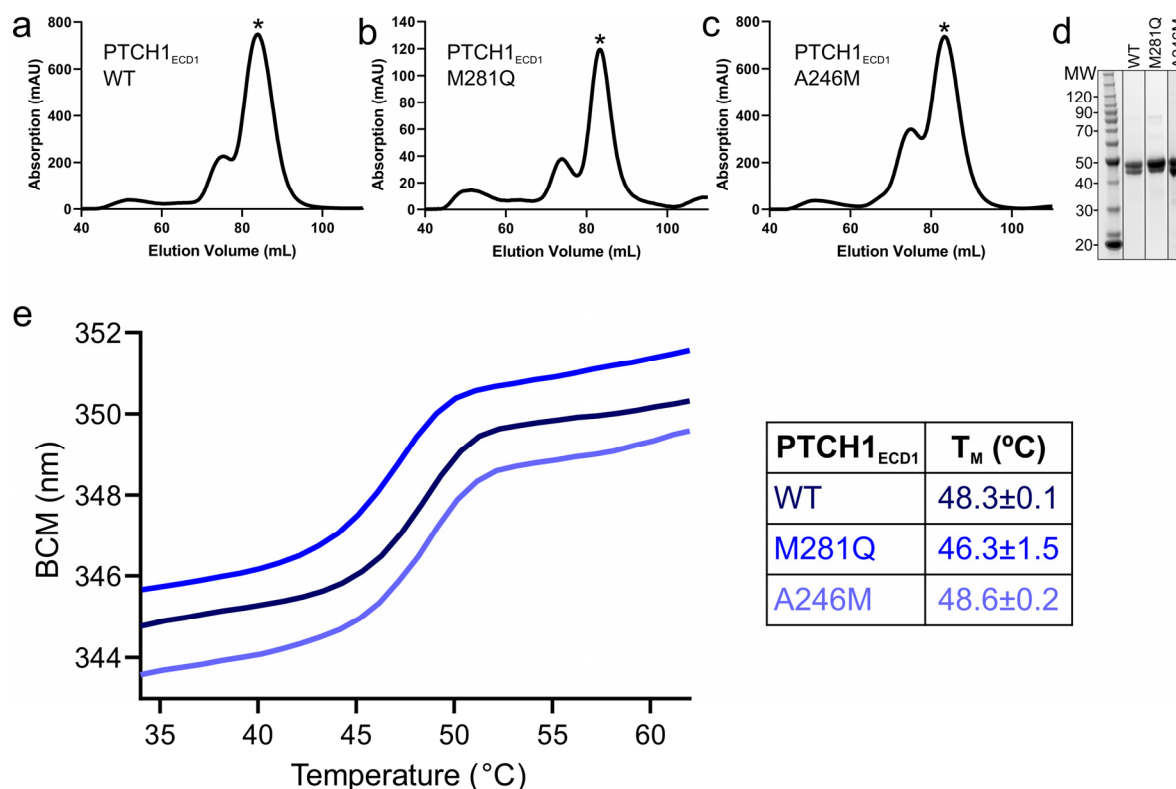


**Supplementary Figure 6: Structural and functional characterisation of PTCH1 cancer mutations.** **a**, PTCH1 mutations mapped onto the human PTCH1 structure reveals hotspots. Mutated residues are shown as spheres and divided into four subtypes: mutations located in ECD1 (pink), ECD2 (green), the sterol sensing domain (SSD, blue) and residual transmembrane domain (TMD, grey). The right panel is 90° rotated around the y axis compared to the left panel. The black box highlights the position of the potential ion binding site (see **h**). **b and c**, Disease mutations prevent secretion of isolated PTCH1<sub>ECD1</sub> and PTCH1<sub>ECD2</sub> proteins from HEK293T cells. Immunoblots show results of tests for both expression (bottom) and secretion (top) for PTCH1<sub>ECD1</sub> (**b**) and PTCH1<sub>ECD2</sub> (**c**) constructs bearing the indicated cancer-associated mutations. Of the 27 mutants tested, only 6 (marked in bold) were secreted. These mainly map to surface exposed residues, whereas the majority of mutations that prevent secretion map to residues that participate in the formation of the hydrophobic core of the ECD1 or ECD2. These experiment were independently repeated 3 times with similar results. **d-g**, MD simulations of full length PTCH1 embedded in a POPC:cholesterol membrane were used to analyze mutations in the PTCH1 SSD. **d and e**, Coarse grained representation (at the end of a 10 µs simulation) shows a high probability of cholesterol localization (black shape) within a cavity surrounded by residues (labeled, see also **a**) altered by disease-causing mutations. Colour-coding represents the averaged cholesterol contacts within 0.6 nm of the PTCH1 surface (from blue: highest to pale-yellow: lowest). **e** is related to **d** by a 90° rotation around the x-axis. The high probability for cholesterol binding to the SSD site was also noted in the PTCH1 cryo-EM structures<sup>4,9-11</sup>. **f and g**, Cartoon representation of the SSD sterol-binding site backmapped<sup>12</sup> from the last frame of the coarse grain simulation after 100 ns of atomistic simulation to obtain high-resolution information about the cholesterol-binding pose. Cholesterol re-orient to form hydrophobic contacts with TM2 and TM4, including with the highly conserved P504 residue, providing support for the sterol-binding pose seen in our structural model (**Fig. 2a**). The position of cholesterol at the start (purple) and after 100 ns atomistic MD simulations (pink) are shown as sticks. Disease-associated residues from **a** are shown as spheres and orientations correspond to **d** and **e**, respectively. **h**, Close-up of the potential TMD ion binding site (marked by the square frame in **a** observed in the SHH-PTCH1 complex (PDB Id. 6DMY<sup>4</sup>). The corresponding 3.6 Å cryo-EM map (EMD-7968<sup>9</sup>) is shown as blue mesh. The extra electron potential map is in binding distance to a cluster of negatively charged (D513, D514 and E1095) and polar side chains from TM helices 4, 5 and 10. These acidic TM residues (present within a GxxxDD motif in TM4 and GxxxE motif in TM10) are conserved in RND family proteins<sup>13</sup> (**i**), where they are thought to mediate proton flux that drives the conformational cycle<sup>14</sup>. Mutations in these residues impair PTCH1 function and have been linked to a familial cancer pre-disposition syndrome (Gorlin's syndrome<sup>10,13</sup>). We speculate that this electron density may represent a sodium ion<sup>15</sup> or other monovalent cation that permeates through the center of the TMD, analogous to the pathway for proton flux recently described for the MmpL3 transporter from mycobacteria<sup>16</sup>. **i**, Sequence alignment of residues forming the potential ion binding site. Sequences are coloured by residue type. TMD residues mutated in cancers are coloured according to **a**. Sequence alignment was performed using T-coffee ([www.ebi.ac.uk/Tools/msa/tcoffee/](http://www.ebi.ac.uk/Tools/msa/tcoffee/)) with manual adjustment based on the position of TM4 and TM10 observed in structures. Sequences were obtained from Uniprot; PTCH1 (Q13635), PTC2 (Q9Y6C5), NPC1 (O15118), AcrB (P31224), MmpL3 (I7G2R2), SecDF(Q5SKE6).

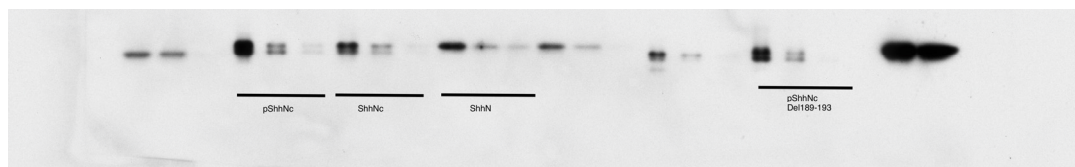


**Supplementary Figure 7: Comparison of PTCH1 to NPC1 and other members of the resistance-nodulation-division (RND) superfamily.** Structures were superimposed using the 12-TM helix domain as a template. All RND family members have a conserved fold consisting of 12 transmembrane helices and two extracellular  $\alpha+\beta$  sandwich domains. However, the top of the ECD is formed by very divergent structural features (highlighted), adding a specific function to each of the proteins. In case of PTCH1 (cyan/blue) these insertions from the cholesterol- and SHH-binding sites, whereas in NPC1 (light yellow/yellow, PDB Id. 5U73<sup>17</sup>) these insertions bind to NPC2. ACRB (light green/green, PDB Id. 1IWG<sup>18</sup>) has a duplicated  $\alpha+\beta$  sandwich domain and uses the insertions for trimerisation and ACRA/TOLC binding. MmpL3 (pink/purple, PDB Id. 6AJF<sup>16</sup>) contains very small insertions in its  $\alpha+\beta$  sandwich domains, whereas in SecDF (wheat/brown, PDB Id. 3AQP<sup>19</sup>) an insertion is only seen in the first  $\alpha+\beta$  sandwich domain, which binds to unfolded protein substrates.

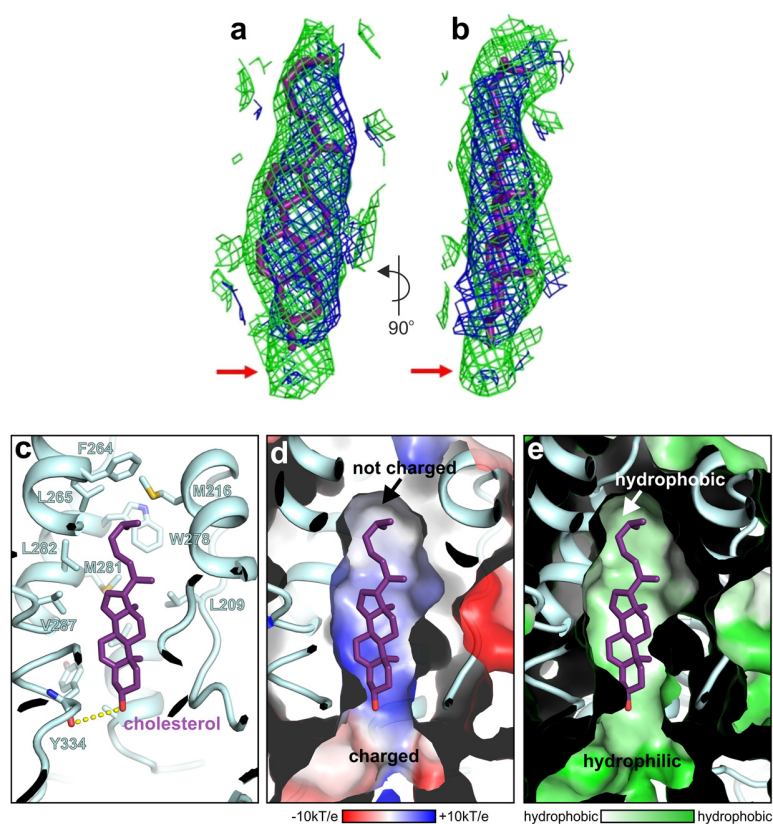




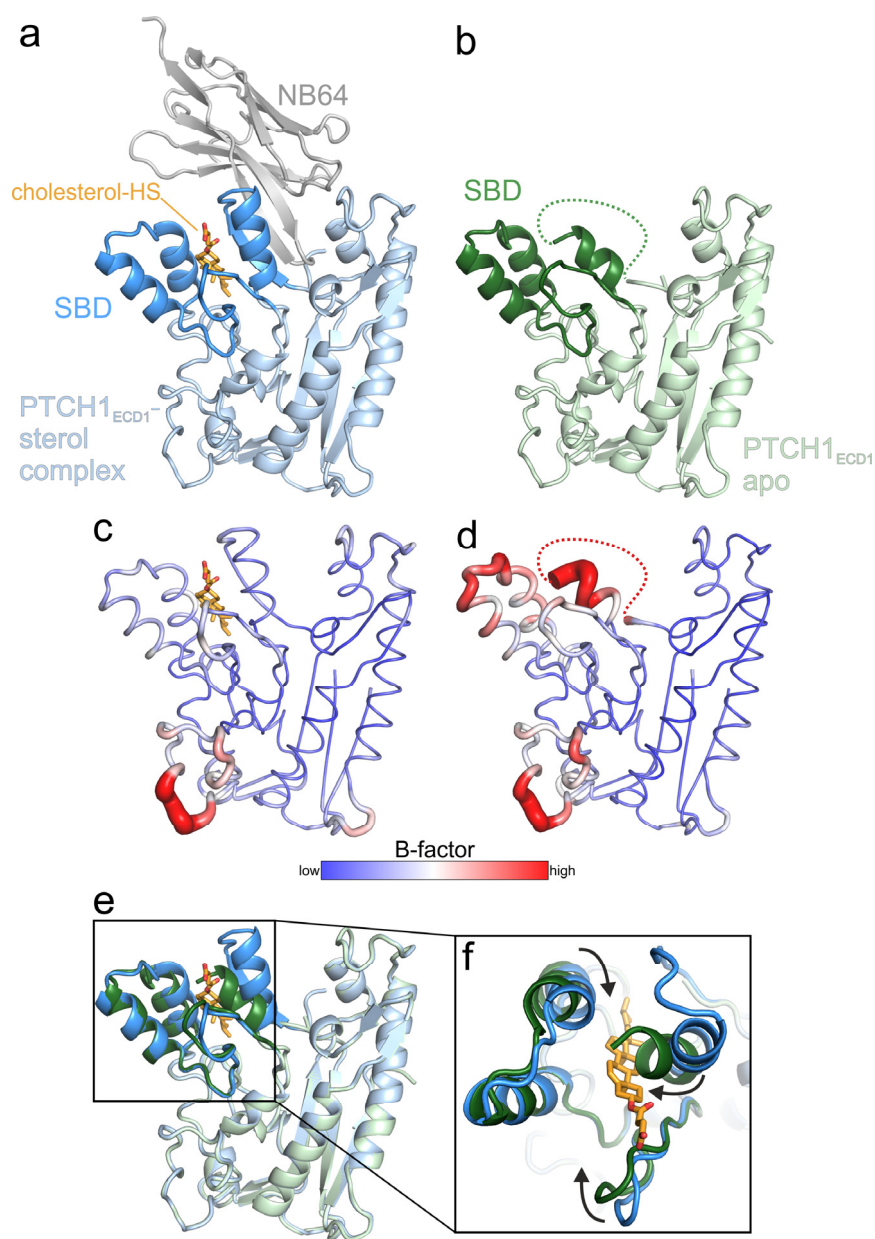
**Supplementary Figure 8: Production and stability of PTCH1<sub>ECD1</sub> wildtype and mutant proteins.** **a-c**, SEC elution profiles of PTCH1<sub>ECD1</sub> WT and the two mutants M281Q and A246M localized in the PTCH1 sterol-binding domain (SBD, see Fig.2). **d**, SDS-PAGE of indicated peak fractions in **a-c** used for ITC experiments shown in **Fig.3d-g**. The expression for the PTCH1<sub>ECD1</sub>-WT was independently repeated 5 times with similar results. The expression of the PTCH1<sub>ECD1</sub>-M281Q and -A246M mutants was repeated 2 times with similar results. **e**, Thermostability analysis of the PTCH1<sub>ECD1</sub> proteins. Representative curves for the thermal unfolding of PTCH1<sub>ECD1</sub> wildtype and mutants are displayed in the graph. Thermostability is monitored using thermal ramping (15°C to 95°C) paired with intrinsic fluorescence. The Barycentric mean (BCM) of the broad-spectra intrinsic fluorescence measurement is calculated and plotted against temperature. The melting temperatures were determined as the arithmetic mean plus/minus one standard deviation derived from 3 independent measurements, with each measurement containing 4 technical replicates.



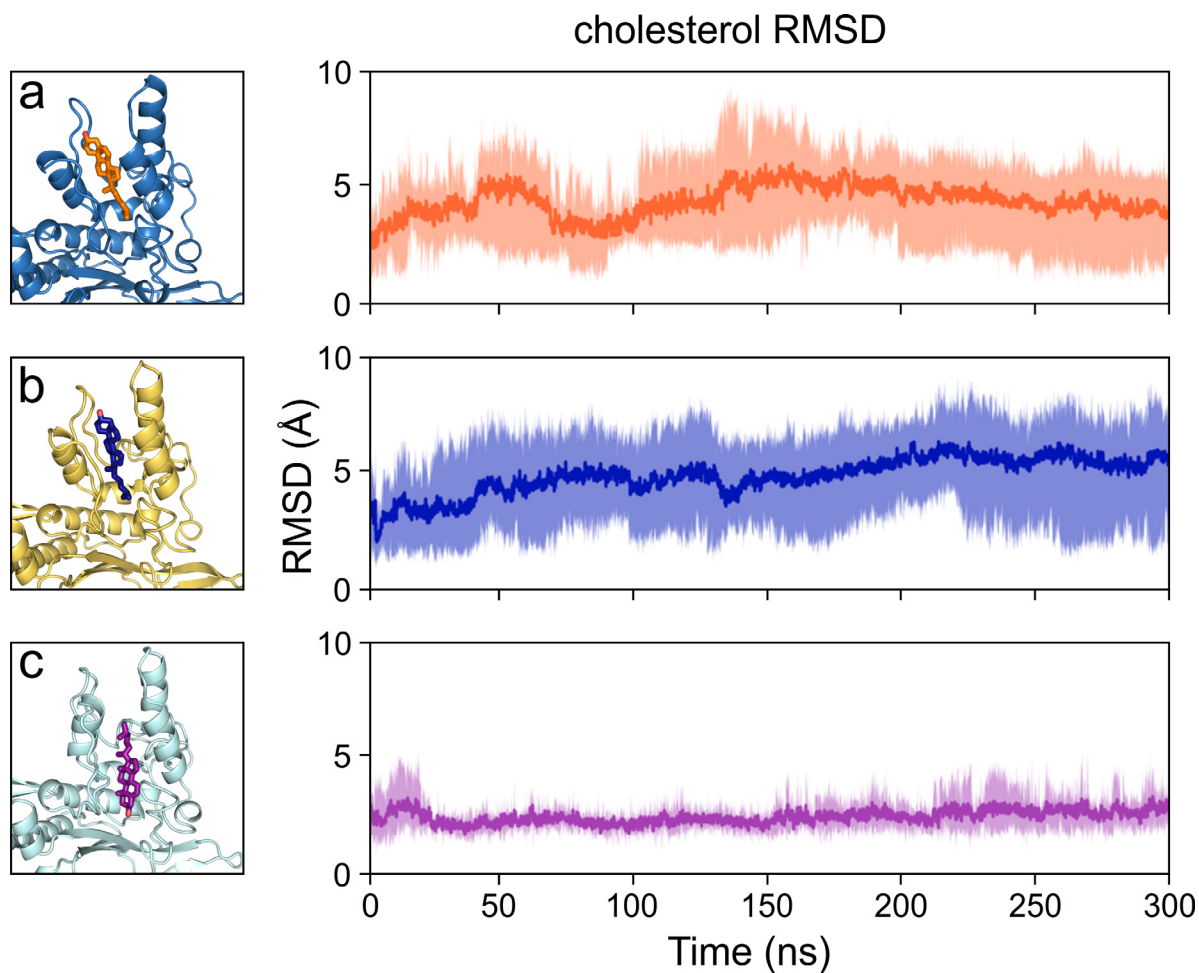
**Supplementary Figure 9: Uncropped scanned image of the western blot from Fig. 4b.**



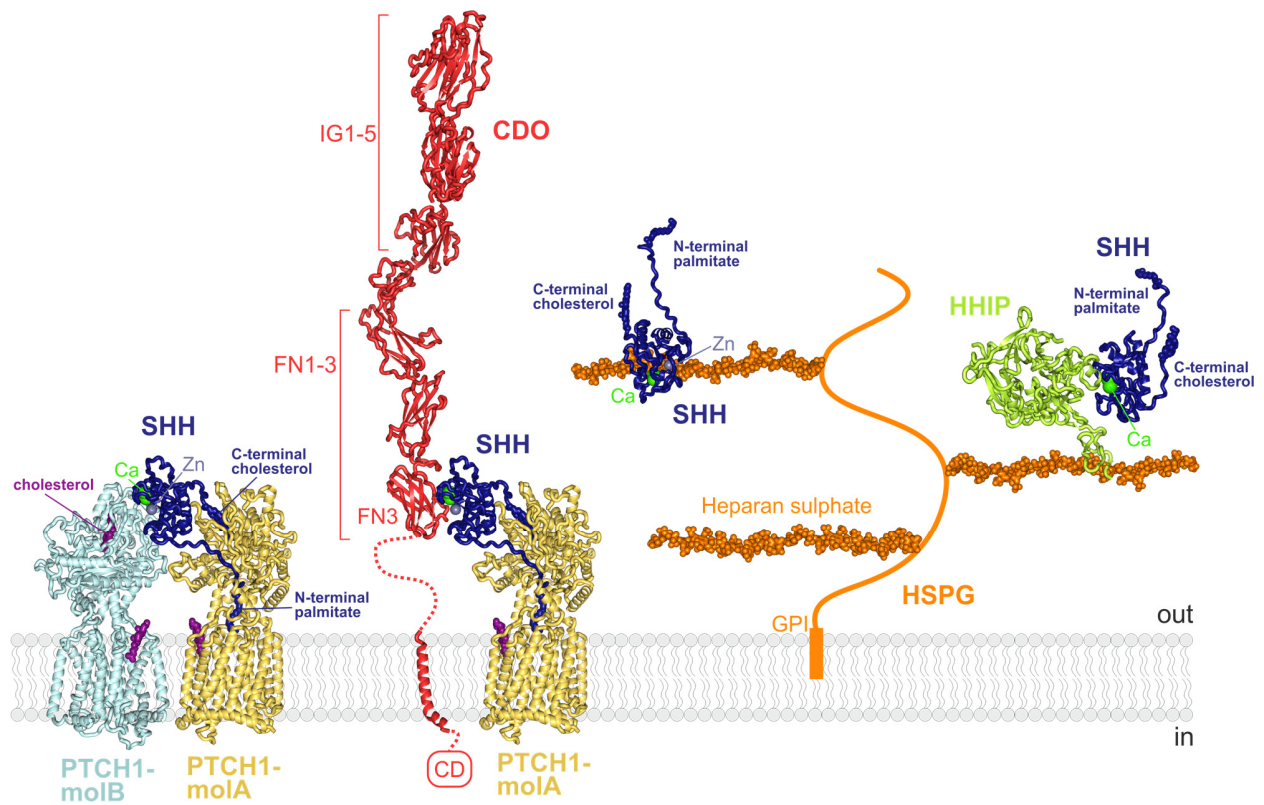
**Supplementary Figure 10: Analysis of the free cholesterol in PTCH1-molB.** **a and b**, Superimposition of the cryo-EM maps EMD-8955<sup>4</sup> (used here for reassessment) and EMD-7968<sup>9</sup> (the 1:1 PTCH1-SHH complex) seen from the face (**a**) and side view (**b**) of the free cholesterol molecule. Cholesterol is shown in sticks and coloured in violet. The cryo-EM maps are coloured in blue (EMD-8955) and green EMD-7968), respectively. The red arrows show the extra density corresponding the hemisuccinate group that is present in the 1:1 PTCH1:SHH complex<sup>9</sup>, but not in the free cholesterol-PTCH1-molB complex in this study. This observation is consistent with the “hydroxyl-down” orientation of cholesterol. **c-e**, Close up view of the Sterol Binding Domain (SBD) in PTCH1-molB. **c**, Stick presentation of interacting residues. Cholesterol is depicted in violet, PTCH1-molB in cyan. F264, M216, L265 and W278 participate in forming a hydrophobic lid, thereby closing the entrance where the SHH-cholesterol inserts in PTCH1-molA. **d**, electrostatic potential mapped onto the solvent accessible surface of PTCH1-molB calculated with APBS (<http://www.poissonboltzmann.org/>) using standard settings in the APBS plugin in PyMOL. The sterol-binding pocket shows an amphiphilic character with non-charged residues forming the lid and charged residues located near the bottom of the mol-B SBD. **e**, Solvent accessible surface of PTCH1-molB coloured according to normalized consensus hydrophobicity scale<sup>20</sup> using standard parameters from PyMOL. The SBP region is hydrophobic whereas the centre, where we placed the  $\beta$ -hydroxyl group of cholesterol, is hydrophilic, thus consistent with the “hydroxyl-down” orientation of the free cholesterol in PTCH1-molB.



**Supplementary Figure 11: Structural plasticity of the PTCH1<sub>ECD1</sub> sterol-binding domain (SBD).** **a and b,** Cartoon representation of PTCH1<sub>ECD1</sub>-NB64-cholesterol-HS complex (**a**) and PTCH1<sub>ECD1</sub> apo (**b**) crystal structures. The SBD is highlighted. Cholesterol-HS is depicted in stick representation. The flexible linker connecting the SBD to the  $\alpha+\beta$  sandwich domain in PTCH1<sub>ECD1</sub> apo is shown as dashed line. **c and d,** Ribbon representations of the PTCH1<sub>ECD1</sub>-NB64-cholesterol hemisuccinate complex (**c**) and the PTCH1<sub>ECD1</sub> apo (**d**) structures coloured according to B factor distribution from blue (low, ordered) to red (high, disordered). The increased relative disorder in the SBD of apo-PTCH1 is clearly discernable. Note that the relatively higher order in the PTCH1<sub>ECD1</sub>-NB64-cholesterol-hemisuccinate complex could be a consequence of both sterol-binding and NB64-binding. Orientations are as in **a** and **b**. **e,** Superposition of the PTCH1 complex and structures from **a** and **b**. Major differences are mostly found in the SBD. **f,** Close-up view of the SBD. A helix in the apo structure collapses into the SBD. The rearrangements are highlighted by arrows.



**Supplementary Figure 12: Orientation dependent stabilisation of cholesterol.** Average RMSD of cholesterol (all atoms) bound to PTCH1<sub>ECD</sub> constructs using 5 x 300 ns atomistic MD simulations of each construct. Left panel: cartoon representation of the sterol-binding site at 0 ns. Right panel: average cholesterol RMSD relative to t=0 ns over the length of the simulation. The range between the minimum and maximum cholesterol RMSD values at each time point within the five repeats is shown as transparent fill. **a**, PTCH1<sub>ECD1</sub> crystal structure. **b**, PTCH1<sub>ECD</sub>-molA refined cryo-EM structure. **c**, PTCH1<sub>ECD</sub>-molB cryo-EM structure.



**Supplementary Figure 13: Model for SHH co-receptor interactions.** Structures of SHH in complex with CDO (red PDB Id. 3D1M<sup>6</sup>), HHIP (green, PDB Id. 2WFX<sup>7</sup>) and the glycosaminoglycan chains of HSPGs (orange, PDB 4C4N<sup>21</sup>) reveal overlap with the protein only interface between SHH and PTCH1-molB (from this study) driven by the SHH calcium and zinc-binding sites. The SHH:PTCH1 1:2 complex is depicted as in Fig. 2a. The CDO:SHH complex model was generated using the HHPRED webserver<sup>22</sup> and combined with the crystal structure of the CDO-FN3:SHH complex (PDB ID. 3D1M<sup>6</sup>). Ig: immunoglobulin-like domain; FN: fibronectin type III-like domain; CD: cytoplasmic domain; GPI: glycosylphosphatidylinositol anchor; HSPG: heparan sulphate proteoglycan.



## REFERENCES

- 1 Murshudov, G. N. *et al.* REFMAC5 for the refinement of macromolecular crystal structures. *Acta Crystallogr D Biol Crystallogr* **67**, 355-367, doi:10.1107/S0907444911001314 (2011).
- 2 BUSTER v. 2.10.2 (Global Phasing Ltd., Cambridge, United Kingdom, 2011).
- 3 Laskowski, R. A., Jablonska, J., Pravda, L., Varekova, R. S. & Thornton, J. M. PDBsum: Structural summaries of PDB entries. *Protein Sci* **27**, 129-134, doi:10.1002/pro.3289 (2018).
- 4 Qi, X., Schmiede, P., Coutavas, E. & Li, X. Two Patched molecules engage distinct sites on Hedgehog yielding a signaling-competent complex. *Science* **362**, doi:10.1126/science.aas8843 (2018).
- 5 Beachy, P. A., Hymowitz, S. G., Lazarus, R. A., Leahy, D. J. & Siebold, C. Interactions between Hedgehog proteins and their binding partners come into view. *Genes Dev* **24**, 2001-2012, doi:10.1101/gad.1951710 (2010).
- 6 McLellan, J. S. *et al.* The mode of Hedgehog binding to Ihog homologues is not conserved across different phyla. *Nature* **455**, 979-983 (2008).
- 7 Bishop, B. *et al.* Structural insights into hedgehog ligand sequestration by the human hedgehog-interacting protein HHIP. *Nat Struct Mol Biol* **16**, 698-703 (2009).
- 8 Bosanac, I. *et al.* The structure of SHH in complex with HHIP reveals a recognition role for the Shh pseudo active site in signaling. *Nat Struct Mol Biol* **16**, 691-697 (2009).
- 9 Gong, X. *et al.* Structural basis for the recognition of Sonic Hedgehog by human Patched1. *Science* **361**, doi:10.1126/science.aas8935 (2018).
- 10 Zhang, Y. *et al.* Structural Basis for Cholesterol Transport-like Activity of the Hedgehog Receptor Patched. *Cell* **175**, 1352-1364 e1314, doi:10.1016/j.cell.2018.10.026 (2018).
- 11 Qi, X., Schmiede, P., Coutavas, E., Wang, J. & Li, X. Structures of human Patched and its complex with native palmitoylated sonic hedgehog. *Nature* **560**, 128-132, doi:10.1038/s41586-018-0308-7 (2018).
- 12 Stansfeld, P. J. & Sansom, M. S. From Coarse Grained to Atomistic: A Serial Multiscale Approach to Membrane Protein Simulations. *Journal of chemical theory and computation* **7**, 1157-1166, doi:10.1021/ct100569y (2011).
- 13 Taipale, J., Cooper, M. K., Maiti, T. & Beachy, P. A. Patched acts catalytically to suppress the activity of Smoothened. *Nature* **418**, 892-897, doi:10.1038/nature00989 (2002).
- 14 Guan, L. & Nakae, T. Identification of essential charged residues in transmembrane segments of the multidrug transporter MexB of *Pseudomonas aeruginosa*. *J Bacteriol* **183**, 1734-1739, doi:10.1128/JB.183.5.1734-1739.2001 (2001).
- 15 Myers, B. R., Neahring, L., Zhang, Y., Roberts, K. J. & Beachy, P. A. Rapid, direct activity assays for Smoothened reveal Hedgehog pathway regulation by membrane cholesterol and extracellular sodium. *Proc Natl Acad Sci U S A* **114**, E11141-E11150, doi:10.1073/pnas.1717891115 (2017).
- 16 Zhang, B. *et al.* Crystal Structures of Membrane Transporter MmpL3, an Anti-TB Drug Target. *Cell* **176**, 636-648 e613, doi:10.1016/j.cell.2019.01.003 (2019).
- 17 Li, X. *et al.* 3.3 A structure of Niemann-Pick C1 protein reveals insights into the function of the C-terminal luminal domain in cholesterol transport. *Proc Natl Acad Sci U S A* **114**, 9116-9121, doi:10.1073/pnas.1711716114 (2017).
- 18 Murakami, S., Nakashima, R., Yamashita, E. & Yamaguchi, A. Crystal structure of bacterial multidrug efflux transporter AcrB. *Nature* **419**, 587-593, doi:10.1038/nature01050 (2002).
- 19 Tsukazaki, T. *et al.* Structure and function of a membrane component SecDF that enhances protein export. *Nature* **474**, 235-238, doi:10.1038/nature09980 (2011).
- 20 Eisenberg, D., Schwarz, E., Komaromy, M. & Wall, R. Analysis of Membrane and Surface Protein Sequences with the Hydrophobic Moment Plot. *J Mol Biol* **179**, 125-142, doi:10.1016/0022-2836(84)90309-7 (1984).
- 21 Whalen, D. M., Malinauskas, T., Gilbert, R. J. & Siebold, C. Structural insights into proteoglycan-shaped Hedgehog signaling. *Proc Natl Acad Sci U S A* **110**, 16420-16425, doi:10.1073/pnas.1310097110 (2013).
- 22 Zimmermann, L. *et al.* A Completely Reimplemented MPI Bioinformatics Toolkit with a New HHpred Server at its Core. *J Mol Biol* **430**, 2237-2243, doi:10.1016/j.jmb.2017.12.007 (2018).